inorganics

MDPI

Article

Synthesis, Characterization, and Cytotoxicity of a Ga(III) Complex with Warfarin

Hubert Joe [1], Venceslava Atanasova [2], Jan Mojžiš [3] and Irena Kostova [2,*]

[1] Department of Nanoscience & Nanotechnology, University of Kerala, Trivandrum 695581, India; hubertjoe@keralauniversity.ac.in
[2] Department of Chemistry, Faculty of Pharmacy, Medical University, 2 Dunav St., 1000 Sofia, Bulgaria; venceslava.atanasova8@gmail.com
[3] Department Pharmacology, Faculty of Medicine, P.J. Šafarik University, 040 01 Košice, Slovakia; jan.mojzis@upjs.sk
* Correspondence: irenakostova@yahoo.com

Abstract: The gallium(III) complex of warfarin was synthesized, and its structure was determined by means of theoretical, analytical, and spectral analyses. Significant differences in the IR and Raman spectra of the complex were observed as compared to the spectra of the ligand and confirmed the suggested metal-ligand binding mode. The theoretical study of the Ga(III) complex of warfarin has been done to elucidate the structure-activity relation, inter- and intra-molecular interactions, and frontier molecular orbital energy analysis based on DFT computations. A molecular docking study has been performed to predict the biological activity of the molecule. In this paper, we report preliminary results about the cytotoxicity of the investigated compounds. The cytotoxic effects of the ligand and its Ga(III) complex were determined using the MTT method on different tumor cell lines. The screening performed revealed that the tested compounds exerted cytotoxic activity on the evaluated cell lines.

Keywords: warfarin; Ga(III) complex; DFT; vibrational spectroscopy; cytotoxicity

check for updates

Citation: Joe, H.; Atanasova, V.; Mojžiš, J.; Kostova, I. Synthesis, Characterization, and Cytotoxicity of a Ga(III) Complex with Warfarin. *Inorganics* **2024**, *12*, 177. https://doi.org/10.3390/inorganics12070177

Academic Editor: Vladimir Arion

Received: 20 May 2024
Revised: 8 June 2024
Accepted: 20 June 2024
Published: 24 June 2024

Copyright: © 2024 by the authors. Licensee MDPI, Basel, Switzerland. This article is an open access article distributed under the terms and conditions of the Creative Commons Attribution (CC BY) license (https://creativecommons.org/licenses/by/4.0/).

1. Introduction

Coumarin derivatives have attracted considerable interest because of their various physiological and biochemical properties as anticoagulants, spasmolytics, cytotoxic, and anticancer drugs [1,2]. Coumarins exist in a variety of forms due to the various substitutions possible in their basic structure, which modulate their biological activity. The coumarin ring system has an easy acceptability in the biological system compared to its isomeric chromone and flavone nucleus and is widely distributed in nature.

Warfarin (Figure 1) is a popular synthetic anticoagulant that acts by inhibiting the synthesis of vitamin K-dependent coagulation factors and is used in the prevention and treatment of venous thromboembolism. Furthermore, warfarin sodium has been used for the treatment of a variety of cancers and has been shown to improve tumor response rates. However, despite numerous studies, little information has been acquired on the cellular mechanism of action of coumarin compounds in the treatment of malignancies. Therefore, a comprehensive structure-activity relationship study of coumarins with special reference to carcinogenicity, mutagenicity, and cancer-preventing activity would be of high interest [3,4].

Moreover, hydroxycoumarins are phenolic compounds able to act as potent metal chelators and free radical scavengers. Their complexation ability with respect to different metal ions has been studied and discussed widely in a considerable number of investigations [5–8]. We have recently synthesized lanthanide complexes with a number of biologically active coumarins, and we reported their significant antioxidant and cytotoxic activity in different human cell lines [6–8]. It has been found that the binding of a metal

to the coumarin moiety retains or even enhances its biological activity. These promising results prompted us to search for new metal complexes with coumarin ligands. Thus, the aim of this work was to synthesize and characterize a complex of gallium(III) with warfarin in view of determining its cytotoxic activity.

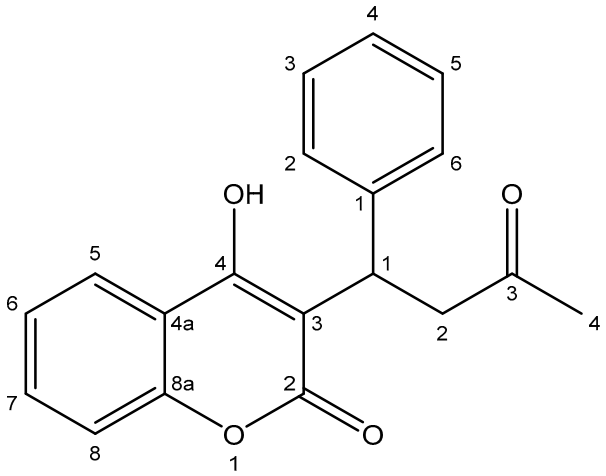


Figure 1. The structure of warfarin.

In recent years, the pharmacological activity of different coumarin derivatives and their metal complexes has been investigated [1–4]. However, more analogs are required to obtain better activity profiles for this class of compounds. These studies highlighted the potential for developing novel complexes, mainly as anticancer therapeutics. This paper represents a further step in such investigations and is concerned with the complex formation of Ga(III) with warfarin. Gallium is the second metal ion, after platinum, to be used in cancer treatment. Its activities are numerous and various. It modifies the three-dimensional structure of DNA and inhibits its synthesis, modulates protein synthesis, and inhibits the activity of a number of enzymes, such as ATPases, DNA polymerases, ribonucleotide reductase, and tyrosine-specific protein phosphatase. Gallium alters plasma membrane permeability and mitochondrial functions [9,10]. It should be noted anyway that exposure to gallium halide complexes can result in acute toxicity. New Ga(III) compounds with better bioavailability are now under clinical investigation and could improve the anticancer and antioxidant activity first demonstrated with Ga(III) nitrate or Ga(III) chloride. Peng et al. have summarized the anticancer mechanisms of Ga(III) and introduced numerous Ga(III) complexes with great antineoplastic potential [10]. Ga(III) salts and metal-based drugs incorporating Ga(III) have been researched as promising antineoplastic agents [11–15] because of the strong resemblances between the gallium(III) and iron(III) cations in terms of electronegativity, ionic radius, coordination polyhedral structures, electro- and Lewis base affinity. Gallium(III) possesses a stable valency in biological conditions, different from Fe(III). Since tumor cells, compared to normal cells, need Fe(III) in larger amounts [16], the inclusion of gallium(III) appears to be a promising strategy in anticancer therapy to disturb the Fe-dependent metabolic pathways in cancer cells [17,18]. Gallium(III) salts, such as, gallium nitrate, chloride, and citrate, have been studied for their anticancer, anti-inflammatory, antimicrobial, etc. properties [19]. Numerous Ga(III) complexes have been investigated in the last few years for their pharmacological activity [11–14,20].

This work is a continuation of the author's work in studying the ligand warfarin and developing its metal complexes; please see the references [2–4]. Unfortunately, X-ray diffraction data for all the reported metal complexes of warfarin are not available. Our attempts to obtain suitable crystals for X-rays were unsuccessful because of the low solubility of the complexes. Therefore, we undertook a combined theoretical and experimental study aiming to determine the binding mode of the ligand and the molecular geometry of its complexes.

In the present investigation, a vibrational spectroscopic study of the anticancer active molecule of the Ga(III) complex of warfarin (WG) has been carried out to elucidate structure–activity relations, inter- and intra-molecular interactions, and frontier molecular orbital energy analysis based on DFT computations. A molecular docking study has been performed to predict the biological activity of the molecule. The synthesis of the Ga(III) complex with warfarin is taken into consideration with cytotoxic screening and further pharmacological study. The cytotoxic effects of the ligand and its Ga(III) complex were determined using the MTT method using different tumor cell lines. Our preliminary tests have shown that the complex reveals promising pharmacologic properties.

2. Materials and Methods

2.1. Synthesis

The compounds used for preparing the solutions were Merck products, p.a. grade. The sodium salt of warfarin was used for the preparation of the metal complex as a ligand. The Ga(III) complex was synthesized by mixing water solutions of $Ga(NO_3)_3$ and the ligand (warfarin sodium) in amounts equal to metal/ligand molar ratio of 1:3. A quantity of 3 mmol of sodium salt of warfarin was dissolved in water. Then, with stirring, an aqueous solution of $Ga(NO_3)_3$ (1 mmol) was added dropwise. The product precipitated, and a fine amorphous powder was obtained immediately. The reaction mixture was stirred with an electromagnetic stirrer at room temperature for one hour. The precipitate was separated by filtration, washed with water, and dried in a desiccator to a constant weight (yield of 86%).

2.2. Analytical and Spectroscopic Measurements

The carbon and hydrogen were determined using elemental analysis. The metal ion and water content were determined using DTA, TGA, and Karl Fisher analysis. The elemental analysis data of the Ga(III) complex obtained is in agreement with the formula, $Ga(L)_3.3H_2O$ ($L = C_{19}H_{15}O_4^-$). Found/Calculated (%): C, 65.07/65.45; H, 4.79/4.88; Ga, 6.58/6.69; H_2O, 5.52/5.17. DTA and TGA analyses were carried out using a derivatograph produced by MOM (Hungary). Samples smaller than 0.25 mm were placed in platinum crucibles. The heating rate was 10 °C min^{-1} up to 900 °C. The inert substance was Al_2O_3. The clearly manifested endothermic peak (100 °C) at the beginning of the DTA curve and the steady mass loss recorded correspond to the elimination of 3 molecules of water per molecule of the Ga(III) complex. This mass loss, determined also using the Karl Fisher analysis, is correlated with the intensity of endothermic effects and with the respective mass decreases. On heating the complex, the decomposition step corresponds to the loss of ligand molecules, which is in agreement with the proposed composition of the complex. The exothermic effect (500 °C) dominates in the thermogram of the complex, resulting from the decomposition of organic matter. A further mass loss recorded up to 750 °C indicates the formation of a thermally stable metal oxide.

The FT-IR spectrum of the Ga(III) complex of warfarin was recorded in KBr (4000–400 cm^{-1}) using an IFS25 Bruker spectrometer with a resolution of 1 cm^{-1} and a FT-IR Equinox 55 Bruker spectrometer with an attenuated total reflectance (ATR) module. An integrated FRA-106 S Raman module was employed for recording the FT-Raman spectrum, using a Nd:YAG laser operating at a 1064 nm line for excitation. The laser power was 300 mW, and 50 scans were collected for each spectrum. The detection of the Raman signal was carried out with a nitrogen-cooled Ge detector. The spectral resolution was 2 cm^{-1}.

2.3. Tumor Cell Lines

Jurkat (human T-cell acute lymphoblastic leukemia), HeLa (human cervical adenocarcinoma), MCF-7 (human breast adenocarcinoma, estrogen receptor-positive), MDA-MB-231 (human breast adenocarcinoma, estrogen receptor-negative), and A-549 cell lines (human lung adenocarcinoma) were kindly provided by Dr. M. Hajdúch (Olomouc, Czech Republic). The CCRF-CEM cell line (human T-cell acute lymphoblastic leukemia) was obtained from the German Collection of Microorganisms and Cell Cultures (Braunschweig,

Germany) The cells were routinely maintained in RPMI 1640 medium with L-Glutamine and HEPES (Jurkat, HeLa, and CCR-CEM) or Dulbecco's modified Eagle's medium with Glutamax-I (MCF-7, MDA-MB-231, and A-549) supplemented with 10% fetal calf serum, penicillin (100 IU $\times$ mL^{-1}), and streptomycin (100 µg $\times$ mL^{-1}) (all from Invitrogen, (Carlsbad, CA, USA), in humidified air with 5% CO_2 at 37 °C. Before each cytotoxicity assay, cell viability was determined using the trypan blue exclusion method and found to be greater than 95%.

2.4. Cytotoxicity Assay

The cytotoxic effects of compounds were determined using a colorimetric microculture assay with the MTT endpoint [21]. Briefly, 3×10^3 (A-549, MCF-7, MDA-MB-231), 5×10^3 (HeLa), or 1×10^4 (Jurkat and CEM) cells were plated per well in 96-well polystyrene microplates (Sarstedt, Germany) in the culture medium containing tested chemicals at final concentrations of 10^{-4}–10^{-9} $mol.L^{-1}$. After 72 h of incubation, 10 µL of MTT (5 mg $\times$ mL^{-1}) (Sigma, Darmstadt, Germany) were added to each well. After an additional 4 h, during which insoluble formazan was produced, 100 µL of 10% sodium dodecylsulfate were added to each well, and another 12 h were allowed for the dissolution of formazan. Absorbance was measured at 540 nm using the automated MRX microplate reader (Dynatech Laboratories, Billingshurst, UK). The blank-corrected absorbance of the control wells was taken as 100%, and the results were expressed as a percentage of the control. All experiments were performed in triplicate.

3. Computational Details

The DFT computations were performed at the Becke three-parameter hybrid method using the Lee–Yang–Parr correlation functional [22–24] at the B3LYP/6-311++G(d,p) level of the theory to attain an optimized geometry and the vibrational wavenumbers of normal modes of the Ga(III) complex of warfarin using the Gaussian'09 program package [25]. As suggested by, Rauhut and Pulay [26], a scaling factor of 0.9673 was used to improve the B3LYP calculated wavenumbers.

4. Results and Discussion

4.1. Coordination Ability of Warfarin to Ga(III)

The reaction of Ga(III) and warfarin sodium afforded a complex that is soluble in dimethyl sulfoxide and insoluble in water and in most of the common organic solvents (methanol, ethanol, and acetone).

4.2. Optimized Geometry Analysis

The optimized geometrical structure of the Ga(III) complex of warfarin is illustrated in Figure 2. The calculated structural parameters, such as bond lengths, bond angles, and dihedral angles, of the Ga(III) complex of the warfarin molecule are compared with experimental structural parameters and listed in Table 1. The absence of a negative wavenumber signifies that the structure of the molecule is true global minima. The calculated and observed bond lengths of C9=O17 are 1.300 Å and 1.214 Å, respectively. The shortening of C=O bond length is due to the effect of the crystalline environment. The phenyl C-H bond lengths are found to be 1.084 Å (C25-H30), 1.085 Å (C24-H29), 1.084 Å (C23-H28), 1.085 Å (C22-H27), and 1.083 Å (C21-H26). The slight shortening of the C21-H26 bond length suggests the formation of improper C-H---O hydrogen bonding. Similarly, the O15---H26 (2.405 Å) distance is significantly less than the van der Waals separation between O and H atoms, which also indicates the possibility of C-H---O hydrogen bonding. In methylene, C-H bond lengths of 1.091 Å (C31-H33) and 1.099 Å (C31-H32) are calculated using the DFT method, and the deviation in bond length also shows the presence of an improper C-H---O hydrogen bonding interaction.

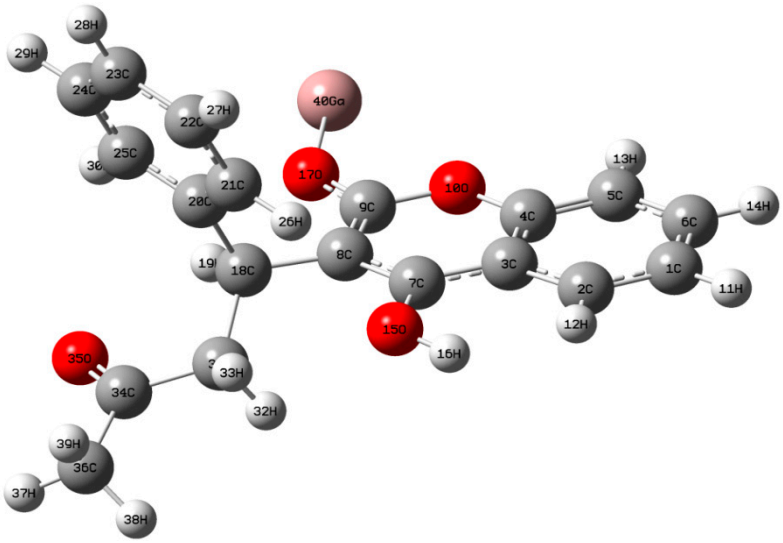


Figure 2. Optimized molecular structure of the Ga(III) complex of warfarin calculated by B3LYP/6-311++G(d,p) level of theory.

Table 1. Structural geometry parameters of the Ga(III) complex of warfarin calculated at B3LYP/6-311++G(d,p) level of theory compared with the single crystal XRD data.

Bond Length (Å)			Bond Angle			Dihedral Angle (°)		
Parameters	**Calc. (Å)**	**XRD (Å)**	**Parameters**	**Calc. (°)**	**XRD (°)**	**Parameters**	**Calc. (°)**	**XRD (°)**
C1-C2	1.391	1.374	C2-C1-C6	120.54	120.03	C6-C1-C2-C3	0.38	−0.22
C1-C6	1.393	1.388	C2-C1-H11	119.44	119.97	C6-C1-C2-H12	−178.76	179.64
C1-H11	1.084	0.951	C6-C1-H11	120.02	120.00	H11-C1-C2-C3	−179.95	179.8
C2-C3	1.417	1.401	C1-C2-C3	121.22	119.85	H11-C1-C2-H12	0.91	−0.34
C2-H12	1.086	0.949	C1-C2-H12	118.32	120.21	C2-C1-C6-C5	0.25	−0.86
C3-C4	1.416	1.382	C3-C2-H12	120.45	119.94	C2-C1-C6-H14	179.97	179.04
C3-C7	1.422	1.449	C2-C3-C4	116.59	119.11	H11-C1-C6-C5	−179.41	−179.12
C4-C5	1.381	1.377	C2-C3-C7	125.41	123.51	H11-C1-C6-H14	0.31	−0.98
C4-O10	1.381	1.378	C4-C3-C7	118.00	117.37	C1-C2-C3-C4	−0.88	1.37
C5-C6	1.402	1.381	C3-C4-C5	122.42	121.32	C1-C2-C3-C7	178.85	−177.67
C5-H13	1.083	0.948	C3-C4-O10	120.17	121.26	H12-C2-C3-C4	178.24	−178.49
C6-H14	1.083	0.953	C5-C4-O10	117.41	117.42	H12-C2-C3-C7	−2.03	2.47
C7-C8	1.416	1.360	C4-C5-C6	119.64	119.01	C2-C3-C4-C5	0.80	−1.48
C7-O15	1.375	1.351	C4-C5-H13	119.01	120.49	C2-C3-C4-O10	−178.91	178.43
C8-C9	1.379	1.443	C6-C5-H13	121.35	120.5	C7-C3-C4-C5	−178.95	177.61
C8-C18	1.527	1.506	C1-C6-C5	119.58	120.66	C7-C3-C4-O10	1.33	−2.48
C9-O10	1.386	1.381	C1-C6-H14	120.56	119.65	C2-C3-C7-C8	179.41	178.63
C9-O17	1.300	1.214	C5-C6-H14	119.86	119.69	C2-C3-C7-O15	0.20	−0.26
O15-H16	0.963	-	C3-C7-C8	121.37	121.74	C4-C3-C7-C8	−0.87	−0.42
O17-Ga40	1.922	-	C3-C7-O15	120.50	123.9	C4-C3-C7-O15	179.93	−179.31
C18-H19	1.090	0.949	C8-C7-O15	118.13	114.35	C3-C4-C5-C6	−0.20	0.43
C18-C20	1.530	1.518	C7-C8-C9	117.64	118.78	C3-C4-C5-H13	179.94	−179.51
C18-C31	1.543	1.545	C7-C8-C18	125.43	122.53	O10-C4-C5-C6	179.52	−179.49
C20-C21	1.401	1.388	C9-C8-C18	116.92	118.4	O10-C4-C5-H13	−0.34	0.57
C20-C25	1.399	1.392	C8-C9-O10	122.33	118.63	C3-C4-O10-C9	−0.79	−0.51
C21-C22	1.393	1.385	C8-C9-O17	126.20	125.38	C5-C4-O10-C9	179.48	179.41
C21-H26	1.083	0.949	O10-C9-O17	111.47	115.97	C4-C5-C6-C1	−0.34	0.76

Table 1. *Cont.*

Bond Length (Å)			Bond Angle			Dihedral Angle (°)		
Parameters	**Calc. (Å)**	**XRD (Å)**	**Parameters**	**Calc. (°)**	**XRD (°)**	**Parameters**	**Calc. (°)**	**XRD (°)**
C22-C23	1.395	1.387	C4-O10-C9	120.47	121.69	C4-C5-C6-H14	179.94	−179.14
C22-H27	1.085	0.951	C7-O15-H16	109.64	-	H13-C5-C6-C1	179.51	−179.31
C23-C24	1.393	1.372	C9-O17-Ga40	131.75	-	H13-C5-C6-H14	−0.21	0.79
C23-H28	1.085	0.950	C8-C18-H19	105.43	107.96	C3-C7-C8-C9	−0.16	6
C24-C25	1.395	1.383	C8-C18-C20	112.75	115.13	C3-C7-C8-C18	−179.00	179.7
C24-H29	1.085	0.952	C8-C18-C31	114.18	109.21	O15-C7-C8-C9	179.07	−175.22
C25-H30	1.084	0.951	H19-C18-C20	106.14	108.28	O15-C7-C8-C18	0.23	−1.53
C31-H32	1.099	0.951	H19-C18-C31	105.63	108.11	C3-C7-O15-H16	−11.02	-
C31-H33	1.091	0.950	C20-C18-C31	111.89	107.95	C8-C7-O15-H16	169.75	-
C31-C34	1.525	1.502	C18-C20-C21	122.10	122.24	C7-C8-C9-O10	0.76	−8.8
C34-O35	1.213	1.290	C18-C20-C25	119.56	119.34	C7-C8-C9-O17	−178.90	−172.64
C34-C36	1.516	1.510	C21-C20-C25	118.34	118.24	C18-C8-C9-O10	179.70	177.24
C36-H37	1.090	0.948	C20-C21-C22	120.74	120.68	C18-C8-C9-O17	0.04	−1.32
C36-H38	1.094	0.951	C20-C21-H26	119.74	119.57	C7-C8-C18-H19	−158.84	−106.78
C36-H39	1.096	0.952	C22-C21-H26	119.52	119.74	C7-C8-C18-C20	85.80	132.15
			C21-C22-C23	120.37	120.12	C7-C8-C18-C31	−43.36	10.54
			C21-C22-H27	119.64	119.9	C9-C8-C18-H19	22.31	66.94
			C23-C22-H27	119.98	119.98	C9-C8-C18-C20	−93.05	−54.14
			C22-C23-C24	119.39	119.8	C9-C8-C18-C31	137.80	−175.74
			C22-C23-H28	120.28	120.14	C8-C9-O10-C4	−0.30	6.17
			C24-C23-H28	120.33	120.06	O17-C9-O10-C4	179.40	−175.14
			C23-C24-C25	120.16	120.02	C8-C9-O17-Ga40	175.02	-
			C23-C24-H29	120.13	119.97	O10-C9-O17-Ga40	−4.67	-
			C25-C24-H29	119.71	120.01	C8-C18-C20-C21	−57.85	−28.35
			C20-C25-C24	120.99	121.21	C8-C18-C20-C25	122.66	156.58
			C20-C25-H30	119.13	119.44	H19-C18-C20-C21	−172.78	−149.25
			C24-C25-H30	119.88	119.44	H19-C18-C20-C25	7.73	35.68
			C18-C31-H32	109.99	108.67	C31-C18-C20-C21	72.48	93.93
			C18-C31-H33	112.14	108.69	C31-C18-C20-C25	−107.01	−81.14
			C18-C31-C34	113.44	112.71	C8-C18-C31-H32	−35.58	−31.08
			H32-C31-H33	105.47	109.33	C8-C18-C31-H33	81.46	−160.03
			H32-C31-C34	105.62	108.71	C8-C18-C31-C34	−153.61	−39.48
			H33-C31-C34	109.67	108.69	H19-C18-C31-H32	79.79	−161.7
			C31-C34-O35	122.60	108.17	H19-C18-C31-H33	−163.18	−42.81
			C31-C34-C36	115.84	114.09	H19-C18-C31-C34	−38.25	77.75
			O35-C34-C36	121.54	113.17	C20-C18-C31-H32	−165.16	−44.77
			C34-C36-H37	110.26	104.38	C20-C18-C31-H33	−48.13	74.12
			C34-C36-H38	111.18	110.89	C20-C18-C31-C34	76.80	−165.33
			C34-C36-H39	108.80	110.82	C18-C20-C21-C22	−179.76	−174.61
			H37-C36-H38	110.34	110.77	C18-C20-C21-H26	0.46	5.46
			H37-C36-H39	109.17	110.69	C25-C20-C21-C22	−0.26	0.52
			H38-C36-H39	106.99	109.27	C25-C20-C21-H26	179.95	−179.42

The linear fitting plots are given in Figure 3. The correlation coefficients (R^2) were calculated to be 0.974 and 0.916 for the bond length and the bond angle, respectively, as compared with the experimental values. It shows a good agreement between the calculated and observed values.

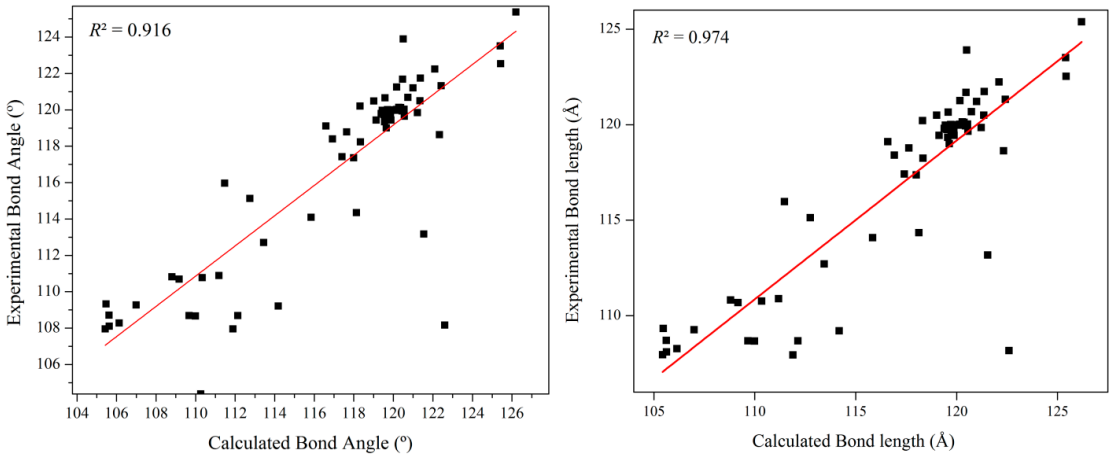


Figure 3. Correlation plot for computational and experimental bond angle (**left**) and bond length (**right**) of the Ga(III) complex of warfarin.

4.3. Natural Bond Orbital Analysis

NBO analysis was performed on the molecule using the NBO 3.1 program (Glendening 1998) as implemented in the Gaussian'09 program package at the DFT level in order to elucidate the delocalization of ED within the molecule. The corresponding results have been tabulated in Table 2. The hyperconjugation interaction between LP(Ga40)→σ*(C9-O17) shows a large stabilization energy value of 60.32 kcal mol^{-1}, and it is due to the bond formation between the Ga metal ion and the coumarin ring. The interaction between LP(O15)→σ*(C21-H26) confirms the formation of C-H---O intramolecular hydrogen bonding.

Table 2. Donor and acceptor interactions results of the Ga(III) complex of warfarin.

Donor	ED [a] (i) (e)	Acceptor	ED [a] (j) (e)	E(2) [b] kcal mol^{-1}	E(j)-E(i) [c] a.u	F(i,j) [d] a.u.
π (C1-C2)	0.87	π*(C3-C7)	0.32	15.93	0.26	0.09
π (C3-C7)	0.89	π*(C8-C9)	0.18	16.38	0.29	0.09
π (C4-C5)	0.88	π*(C3-C7)	0.32	13.28	0.27	0.09
π(C22-C23)	0.83	π*(C20-C21)	0.17	10.39	0.28	0.07
π(C24-C25)	0.83	π*(C20-C21)	0.17	11	0.28	0.07
π(C24-C25)	0.83	π*(C22-C23)	0.17	10.72	0.28	0.07
LP(O15)	0.99	σ*(C3-C7)	0.02	3.05	1.09	0.07
LP(O15)	0.98	π*(C3-C7)	0.32	4.60	0.34	0.06
LP(O15)	0.98	σ*(C21-H26)	0.01	0.32	0.87	0.02
LP(O17)	0.96	σ*(C9-O10)	0.03	1.48	0.97	0.05
LP(O17)	0.95	σ*(C8-C9)	0.02	4.39	0.91	0.08
LP(O17)	0.95	σ*(C9-O10)	0.03	6.35	0.62	0.08
LP(O35)	0.95	σ*(C31-C34)	0.03	8.56	0.64	0.09
LP(O35)	0.95	σ*(C34-C36)	0.03	8.81	0.63	0.1
σ(C1-C2)	0.99	σ*(C3-C7)	0.32	2.39	1.19	0.07
σ(C1-H11)	0.99	σ*(C2-C3)	0.01	2.82	1.02	0.07
σ(C1-H11)	0.99	σ*(C5-C6)	0.01	2.45	1.05	0.06
σ(C2-C3)	0.98	σ*(C4-O10)	0.02	2.40	0.95	0.06
π(C3-C7)	0.89	π*(C4-C5)	0.17	5.17	0.30	0.05
σ(C5-H13)	0.99	σ*(C3-C4)	0.02	3.19	1.02	0.07
σ(C6-H14)	0.99	σ*(C1-C2)	0.01	2.55	1.06	0.07
π(C8-C9)	0.95	π*(C3-C7)	0.32	2.88	0.29	0.04
σ(C8-C18)	0.98	σ*(C9-O10)	0.03	2.83	0.86	0.06
π(C20-C21)	0.82	π*(C22-C23)	0.17	11.31	0.27	0.07
π(C20-C21)	0.82	π*(C24-C25)	0.17	10.50	0.28	0.07

Table 2. *Cont.*

Donor	ED [a] (i) (e)	Acceptor	ED [a] (j) (e)	E(2) [b] kcal mol^{-1}	E(j)-E(i) [c] a.u	F(i,j) [d] a.u.
σ(C21-H26)	0.99	σ*(C20-C25)	0.01	2.93	1.05	0.07
σ(C22-H27)	0.99	σ*(C20-C21)	0.01	2.77	1.05	0.07
σ(C31-H32)	0.97	π* (C34-O35)	0.05	4.07	0.48	0.06
LP (Ga40)	0.99	σ*(C9-O17)	0.02	60.32	0.66	0.05

[a] Electron density. [b] Energy of stabilization interactions. [c] Energy difference between donor and acceptor i and j NBO orbitals. [d] Fock matrix elements between i and j NBO orbitals.

The intramolecular hyperconjugative interactions are formed by the orbital overlap between π(C-C)→π*(C-C) and σ(C-C)→σ*(C-C) and σ*(C-O) bond orbitals, which results in ICT causing stabilization of the system. Rehybridization of corresponding bond contraction and strengthening reveals low electron density in their antibonding orbitals, such as σ*(C2-C3), σ*(C1-C2), and so on. Strong intramolecular hyperconjugative interactions of π-electrons have been noticed in the phenyl ring C-C bonds such as C1-C2→C3-C7 (15.93 kcal mol^{-1}); C3-C7→C8-C9 (16.38 kcal mol^{-1}); C4-C5→C3-C7 (13.28 kcal mol^{-1}).

4.4. Natural Population Analysis

The charge distribution of a molecule has a significant influence on the vibrational spectra. The natural atomic charges were calculated at the B3LYP level using Gaussian'09 with the 6-311++G(d,p) basis set. The natural charge distribution plot of the Ga(III) complex of warfarin is shown in Figure 4. The oxygen atom O17 (−1.01 e) in the coumarin ring system has more negative charge than other oxygen atoms O10 (−0.56 e) and O15 (−0.75 e) due to the bond formation between the metal ions Ga and the oxygen atom O17. The carbon atoms substituted with oxygen atoms such as C4, C7, C9, and C34 exhibit more positive charges in comparison with other carbon atoms in the molecule, and the negative charges are due to sp^3 hybridization presented in the carbon atom.

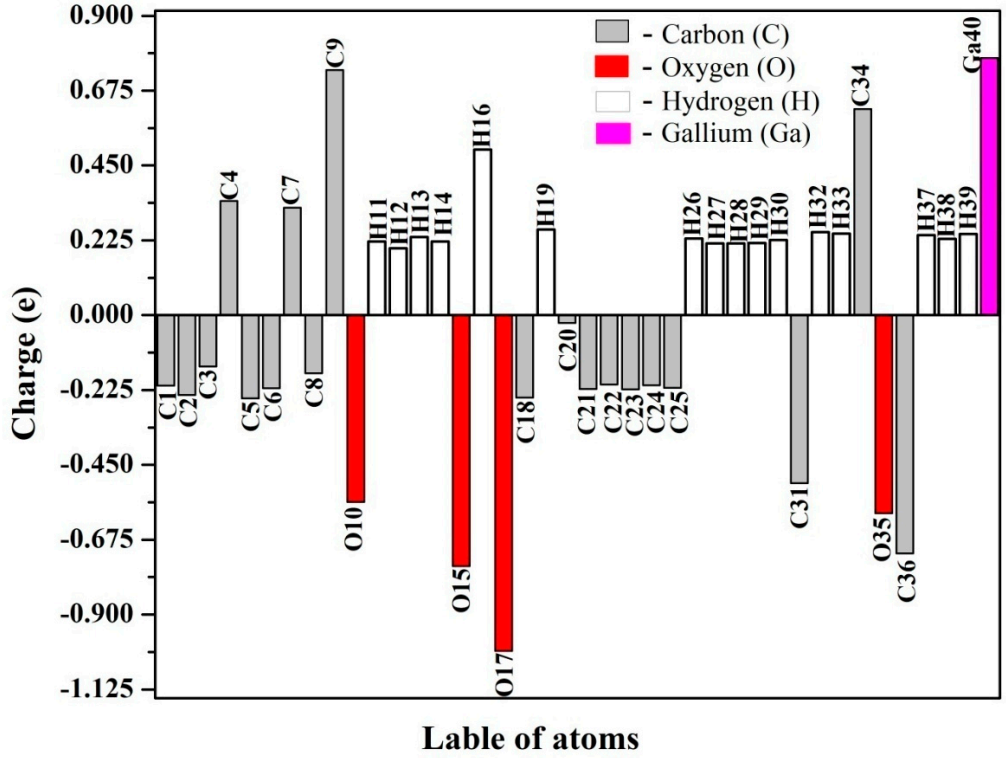


Figure 4. Natural charge distribution chart diagram of the Ga(III) complex of warfarin.

The coumarin-made fused carbon atoms of C3 and C4 possess maximum charges compared with the rest, while C4 shows a positive value due to the strong electronegative oxygen connection. The H16 of hydroxyl shows the highest positive charge among all other hydrogen atoms in the entire molecular system. Due to the donating nature of the methyl group, carbon C36 holds more negative charges than others.

4.5. Vibrational Spectral Analysis

Vibrational spectral analysis was performed based on normal coordinate analysis followed by SQM force field methodology. The experimental FTIR and FT-Raman spectra in comparison with the simulated spectra are given in Figures 5 and 6, respectively. The internal valence coordinates of the molecule are defined based on Pulay's recommendations [27], and they are shown in Table 3. Scaled wavenumbers related to the observed infrared and Raman peaks are presented in Table 4.

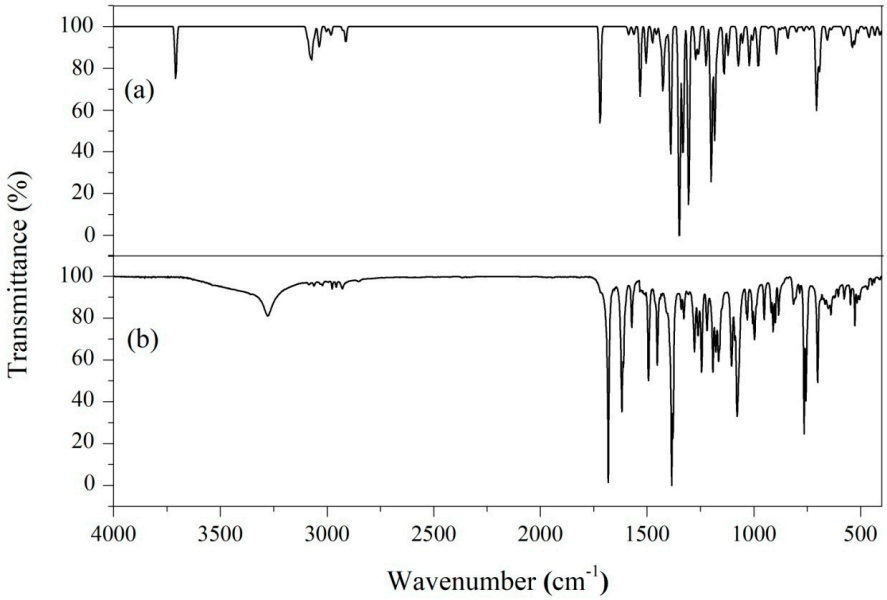


Figure 5. Simulated (**a**) and experimental (**b**) IR spectra of the Ga(III) complex of warfarin.

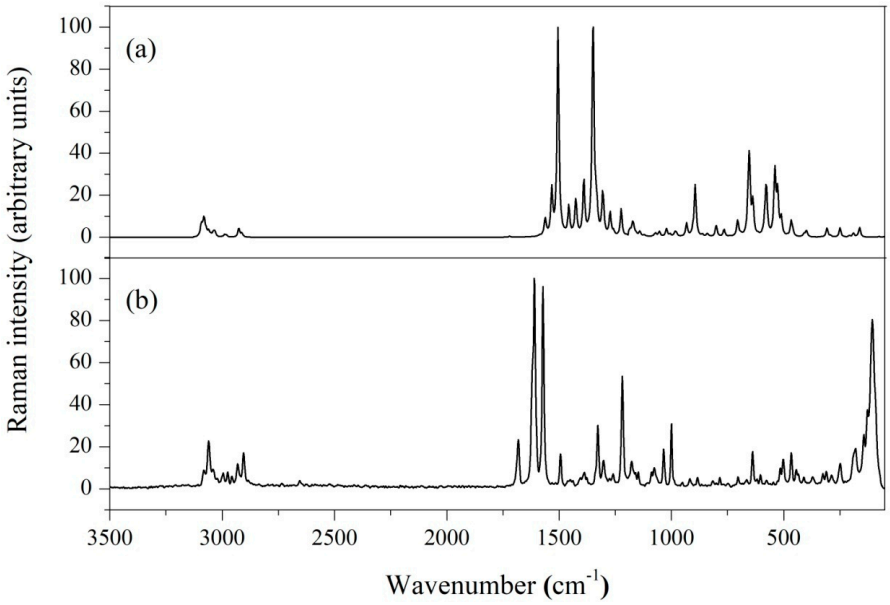


Figure 6. Simulated (**a**) and experimental (**b**) Raman spectra of the Ga(III) complex of warfarin.

Table 3. Definition of internal valence coordinates of the Ga(III) complex of warfarin.

Mode No	Symbol	Type	Definition
		Stretching	
1–12	R_i	C-C (ring)	C1-C2, C2-C3, C3-C4, C4-C5, C5-C6, C6-C1, C20-C21, C21-C22, C22-C23, C23-C24, C24-C25, C25-C20
13–21	r_i	C-H (ring)	C1-H11, C2-H12, C5-H13, C6-H14, C21-H26, C22-H27, C23-H28, C24-H29, C25-H30
22–27	r_i	C-C	C3-C7, C7-C8, C8-C9, C31-C34, C34-C36, C18-C20
28–31	Q_i	C-O (ring)	C9-O10, O10-C4, C9-O17, C7-O15
32	Q_i	C-H	C18-H19
33–34	r_i	C-H (methylene)	C31-H32, C31-H33
35	Q_i	O-GA	O17-Ga40
36	Q_i	C=O	C34-O35
37–38	r_i	C-C	C8-C18, C31-C18
39–41	r_i	C-H (methyl)	C36-H38, C36-H37, C36-H39
42	P_i	O-H	O15-H16
		Bending	
43–60	δ_i	C-C-C (ring)	C6-C1-C2, C1-C2-C3, C2-C3-C4, C3-C4-C5, C4-C5-C6, C5-C6-C1, C7-C3-C4, C3-C4-O10, C4-O10-C9, O10-C9-C8, C9-C8-C7, C8-C7-C3, C25-C20-C21, C20-C21-C22, C21-C22-C23, C22-C23-C24, C23-C24-C25, C24-C25-C20
61–78	β_i	H-C-C (ring)	H11-C1-C6, H11-C1-C2, H12-C2-C1, H12-C2-C3, H14-C6-C5, H14-C6-C1, H13-C5-C4, H13-C5-C6, H26-C21-C20, H26-C21-C22, H27-C22-C21, H27-C22-C23, H28-C23-C22, H28-C23-C24, H29-C24-C23, H29-C24-C25, H30-C25-C24, H30-C25-C20
79–82	β_i	O-C-C (ring)	O15-C7-C8, O15-C7-C3, O17-C9-O10, O17-C9-C8
83–86	β_i	H-C-C	C18-C8-C9, C18-C8-C7, C18-C20-C25, C18-C20-C21
87	δ_i	C-O-Ga (ring)	C9-O17-Ga40
88	β_i	C-O-H (ring)	C7-O15-H16
89	α_i	C-C-C	C31-C34-C36
90–91	β_i	C-C-C	O35-C34-C31, O35-C34-C36
92–94	α_i	H-C-H (methyl)	H37-C36-H39, H38-C36-H37, H38-C36-H39
95–97	β_i	C-C-H (methyl)	C34-C36-H38, C34-C36-H39, C34-C36-H37
98	α_i	H-C-H (methylene)	H32-C31-H33
99	γ_i	C-C-C (methylene)	C18-C31-C34
100	α_i	C-C-C	C8-C18-C31
101	γ_i	H-C-C	H19-C18-C20
102–109	β_i	H-C-C (methylene)	H32-C31-C34, H33-C31-C34, H32-C31-C18, H33-C31-C18, C8-C18-C20, C31-C18-C20, C8-C18-H19, C31-C18-H19
110–111	β_i	*Butt*	C2-C3-C4-O10, C7-C3-C4-C5
		Wagging	
112	ω_i	C-C (ring)	C18-C8-C9-C7
113–114	ω_i	O-C (ring)	O15-C7-C8-C3, O17-C9-O10-C8
115–119	ω_i	C-C	H26-C21-C20-C22, H27-C22-C21-C23, H28-C23-C22-C24, H29-C24-C23-C25, H30-C25-C24-C20
120	ω_i		C18-C20-C25-C21
121–124	ω_i		H11-C1-C6-C2, H12-C2-C1-C3, H14-C6-C5-C1, H13-C5-C4-C6
125	ω_i		O35-C34-C31-C36

Table 3. *Cont.*

Mode No	Symbol	Type	Definition
		Torsion	
126–143	τ_i	tC-C (ring)	C6-C1-C2-C3, C1-C2-C3-C4, C2-C3-C4-C5, C3-C4-C5-C6, C4-C5-C6-C1, C5-C6-C1-C2, C7-C3-C4-O10, C3-C4-O10-C9, C4-O10-C9-C8, O10-C9-C8-C7, C9-C8-C7-C3, C8-C7-C3-C4, C25-C20-C21-C22, C20-C21-C22-C23, C21-C22-C23-C24, C22-C23-C24-C25, C23-C24-C25-C20, C24-C25-C20-C21
144–145	τ_i	tC-O	Ga40-O17-C9-O10, Ga40-O17-C9-C8
146–147	τ_i	tC-O	H16-O15-C7-C3, H16-O15-C7-C8
148–153	τ_i	tC-C	C7-C8-C18-C20, C7-C8-C18-C31, C7-C8-C18-H19, C9-C8-C18-C20, C9-C8-C18-C31, C9-C8-C18-H19
154–159	τ_i	tC-C	C8-C18-C20-C21, C8-C18-C20-C25, C31-C18-C20-C21, C31-C18-C20-C25, H19-C18-C20-C21, H19-C18-C20-C25
160–168	τ_i	tC-C	C8-C18-C31-H32, C8-C18-C31-H33, C8-C18-C31-C34, H19-C18-C31-H32, H19-C18-C31-H33, H19-C18-C31-C34, C20-C18-C31-H32, C20-C18-C31-H33, C20-C18-C31-C34
169–174		tC-C	C18-C31-C34-O35, C18-C31-C34-C36, H32-C31-C34-O35, H32-C31-C34-C36, H33-C31-C34-C36, H33-C31-C34-O35
175–180	τ_i	tC1-C	C31-C34-C36-H38, C31-C34-C36-H37, C31-C34-C36-H39, O35-C34-C36-H38, O35-C34-C36-H37, O35-C34-C36-H38
181–193	τ_i	tC-C	O33-C32-C31-C27, O33-C32-C31-C30, O34-C32-C31-C27, O34-C32-C31-C30, O34-C35-C38-H39, O34-C35-C38-H41, O34-C35-C38-H40, H37-C35-C38-H39, H37-C35-C38-H41, H37-C35-C38-H40, H36-C35-C38-H39, H37-C35-C38-H41, H37-C35-C38-H40

Table 4. The scaled wavenumber obtained at the B3LYP/6-311++G(d,p) level for the normal modes of the Ga(III) complex of warfarin and the assignments proposed for the fundamental bands observed in the experimental IR and Raman spectra.

Scaled Wavenumber (cm^{-1})	Experimental Wavenumber (cm^{-1})		Vibrational Assignment with PED% ($\geq$10)
	IR	Raman	
3710	3278 s	-	ν O15-H16 (100)
3094	-	-	ν C1-H11 (12), ν C5-H13 (33), ν C6-H14 (54)
3089	-	-	ν C21-H26 (80), ν C22-H27 (12),
3082	3085 w	3082 w	ν C1-H11 (29), ν C5-H13 (58), ν C6-H14 (12)
3081	-	-	ν C23-H28 (22), ν C24-H29 (30), ν C25-H30 (36),
3073	-	-	ν C36-H37 (12), ν C36-H38 (40), ν C36-H39 (44)
3071	-	-	ν C1-H11 (53), ν C6-H14 (34)
3062	3062 w	3061 w	ν C22-H27 (42), ν C24-H29 (40), ν C25-H30 (14),
3053	-	-	ν C22-H27 (33), ν C23-H28 (34), ν C24-H29 (27)
3040	-	3041 w	ν C36-H39 (62), ν C36-H37 (23)
3033	3032 w	-	ν C31-H32 (83), ν C31-H33 (12)
	3022 m	-	
3003	-	-	ν C18-H19 (51), ν C31-H33 (46)
2991	2995 w	2995 w	ν C18-H19 (48), ν C31-H33 (47)
2982	2976 w	2976 w	ν C36-H38 (53), ν C36-H39 (42)
	2957 w	2956 w	
2927	2928 w	2931 w	ν C36-H37 (15), ν C36-H38 (32), ν C36-H39 (50)
2914	-	2904 w	ν C31-H32 (93)
	2882 w	2885 w	ν C31-H33 (42)
	2852 w		ν C31-H33 (24)

Table 4. *Cont.*

Scaled Wavenumber (cm^{-1})	Experimental Wavenumber (cm^{-1})		Vibrational Assignment with PED% (≥10)
	IR	Raman	
1721	1757 w	-	ν O35-C34 (89)
	1682 s	1682 m	ν O35-C34 (32)
	1654 s	-	ν O35-C34 (18)
1587	-	1610 s	ν C21-C22 (22), ν C24-C25 (21),
1568	1572 m	1572 s	ν C22-C23 (23), ν C23-C24 (14), ν C20-C25 (14), ν C20-C21 (18)
1562	-	-	ν C4-C5 (24), ν C1-C6 (12), ν C1-C2 (18), ν C3-C4 (17)
1533	-	1531 w	ν C5-C6 (28), δ C2-C1-C6 (12),
1505	-	-	ν C8-C9 (34)
1475	-	-	δ H26-C21-C20 (15), δ H27-C22-C21 (17), δ H29-C24-C25 (16), δ H30-C25-C20 (13)
	-	-	
1457	1453 m	-	δ H12-C2-C3 (12), δ H13-C5-C6 (13)
1437	-	-	ν C21-C22 (10), ν C24-C25 (11), δ H28-C23-C24 (23)
1428	-	-	δ H37-C36-H38 (73), τ C36-H37-C34-H38 (12),
1426	-	-	δ H11-C1-C6 (31), δ H14-C6-C1 (16),
1416	-	-	δ H37-C36-C34 (15), δ H38-C36-H39 (47), τ C36-H38-C34-H39 (27),
1406	-	1404 w	ν C9-O17 (10),
1390	1384 m	1389 w	ν C7-C8 (26), δ H16-O15-C7 (11), δ H19-C18-C8 (16),
1350	1378 m	1377 m	δ H33-C31-C34 (24), OUT C18-C8-C20-H19 (38)
1349	-	-	δ H19-C18-C8 (15),
1338	1340 w	-	δ H37-C36-C34 (12), δ H38-C36-H39 (26), OUT C36-H38-C34-H39 (16),
1332		-	δ H38-C36-H39 (13), ν O15-C7 (11),
1310	1307 w	1302 w	δ H26-C21-C20 (21), δ H30-C25-C20 (19),
1305	-	-	ν C4-C5 (13), ν C1-C6 (17), ν C1-C2 (11), ν C3-C4 (20)
	-	-	
1273	1278 w	1277 w	δ H33-C31-C34 (10), ν O35-C34 (11), δ C8-C9-O10 (10)
1262	1262 w	1260 w	δ C18-C8-C20-H19 (12), δ H32-C31-C18(28),
		-	
1257	1245 w	1242 w	ν C20-C25 (11), δ H12-C2-C3 (10), δ H13-C5-C6 (17), δ H19-C18-C8 (17)
	-		
1224	1219 w	1219 w	δ H12-C2-C3 (14), ν C7-C8 (16); ν O17-C9 (21)
1199	1192 w	-	ν C7-C8 (32), δ H16-O15-C7 (27),
1184	-	-	δ H32-C31-C18(11), ν O10-C4 (21), ν C7-C3 (19)
1173	1178 w	1176 w	δ H37-C36-H38 (16)
1170	-	-	δ H26-C21-C20 (19), δ H27-C22-C21 (16), δ H29-C24-C25 (13), δ H30-C25-C20 (17); ν C1-C2 (25)
1168	1164 w	1159 w	δ H29-C24-C25 (19), δ H28-ν C23-C24 (27),
1158	-	-	δ H33-C31-C34 (10), ν C18-C20 (24)
1142	-	-	δ H27-C22-C21 (11 δ H11-C1-C6 (24), δ H14-C6-C1 (10)
1141	-	-	ν C23-C22 (18); δ H11-C1-C6 (10),
1139	-	-	δ H37-C36-C34 (17), ν C34-C36 (14), ν C31-C34 (10), δ C36-C34-O35 (12)
1121	1104 w	-	δ H13-C5-C6 (20), δ H14-C6-C1 (13), ν O15-C7 (12)
	1089 m	1089 w	
1076	1078 m	1076 w	ν C9-O17 (11), ν C7-O15 (17), δ H14-C6-C1 (12)
1070	-	-	ν C21-C22 (14), ν C24-C25 (15), δ H28-C23-C24 (10)
1053	-	-	ν O15-C7 (10), C18-C31 (21),
1022	-	-	ν C1-C6 (24), ν C5-C6 (11), δ H13-C5-C6 (12),
1020	1030 w	1036 w	ν C22-C23 (19), ν C23-C24 (21)
1006	1006 w	-	OUT C36-H37-C34-H38 (23), δ H32-C31-C18(12)
985	997 w	999 w	C20-C21 (11), δ C22-C23-C24 (26), δ C21-C20-C25 (24),
979	-	-	ν O10-C9 (23),

Table 4. *Cont.*

Scaled Wavenumber (cm^{-1})	Experimental Wavenumber (cm^{-1})		Vibrational Assignment with PED% (≥10)
	IR	Raman	
970	-	-	τ H26-C21-C22-H27 (51), τ H28-C23-C24-H29 (15)
958	952 w	951 w	τ H26-C21-C22-H27 (26), τ H29-C24-C25-H30 (54)
932	-	-	τ C36-H38-C34-H39(11), ν C34-C36 (20), ν C18-C31 (11)
925	919 w	918 w	δ H37-C36-C34 (10); τH11-C1-C6-H14 (74), τ C6-C1-C 5-H14 (10);
905	909 w	-	τ H29-C24-C25-H30 (23), τ H26-C21-C20-C18 (20),
895	899 w	-	τ H28-C23-C24-H29 (15)
876	885 w	883 w	δ H14-C5-C34 (24); τ H13-C5-C6-H14 (78)
862	-	-	τ C36-H37-C34-H38 (13), τ C31-C 18-C34-H32 (10)
842	-	-	δ O10-C9-O17 (11), δ C2-C1-C6 (24)
832	-	-	τ H26-C21-C20-C18 (39), τ H28-C23-C24-H29 (49)
801	814 w	816 w	νC31-C34 (34), ν C34-C36(10)
785	784 w	785 w	τ C6-C1-C5-H14 (30), τ H12-C2-C3-C7(52)
766	765 m	-	τ H28-C23-C24-C25(16), τ C20-C25-C24-C23 (13)
740	755 m	748 w	ν C18-C20 (14), τ C31-C18-C34-H33(10), δ C22-C23-C24 (15)
708	-	-	τ C6-C1-C5-H14 (41), τ H12-C2-C3-C7 (12)
705	701 m	704 w	τ H28-C23-C24-C25 (10), δ C1-C6-C5(10), δ C8-C9-O10 (11)
695	-	-	τ H12-C2-C3-C7 (12), τ C3-C5-O10-C4(47)
691	-	-	τ H28-C23-C24-C25(47), τ C20-C21-C22-C23 (22)
657	666 w	665 w	τ C7-C8-C9-O10(22), τ O17-C8-O10-C9(26)
653	650 w	-	δ C2-C1-C6 (20)
637	639 w	638 w	δ O10-C9-O17 (30), δ C8-C7-O15(11), δ C3-C4-C5 (10)
614	618 w	619 w	δ C23-C24-C25 (75)
584	604 w	603 w	ν C34-C36(16), δ C36-C34-O35 (27)
577	576 w	577 w	δ C22-C23-C24(12), δ C21-C20-C25 (12)
545	547 w	546 w	τ C2-C1-C6-C5 (46), τ O17-C8-O10-C9(11), τ C3-C5-O10-C4(11)
540	-	-	δ C36-C34-O35 (18)
527	526 w	-	τ C22-C23-C24-C25(12),
512	515 w	515 w	τ C18-C21-C25-C20(16)
484	504 w	503 w	τ C2-C1-C6-C5 (13), τ C4-O10-C9-C8(16), τ C2-C3-C7-O15(29)
466	468 w	467 w	δ C3-C7-C8 (28), ν Ga40-O17 (10), τ O35-C31-C36-C34(11)
459	446 w	443 w	τ O35-C31-C36-C34 (33)
433	434 w	436 w	δ C31-C34-C36 (11), τ C22-C23-C24-C25(15)
410	409 w	411 w	τ C1-C2-C3-C4 (20), τ O17-C8-O10-C9(11)
401	-	-	τ C20-C21-C22-C23(45), τ C20-C25-C24-C23(46)
399	-	372 w	νO10-C4(10)
333	-	325 w	τ C1-C2-C3-C4 (33), τ C18-C8-C9-O10(10), τ C2-C3-C7-O15(14)
308	-	310 w	δ C5-C4-O10 (15), δ C8-C7-O15(35)
291	-	287 w	δ C31-C34-C36 (26), δ C20-C18-C31 (19), τ C22-C23-C24-C25(11)
252	-	-	τ C6-C5-C4-O10 (61)
250	-	249 w	δ C5-C4-O10 (24), ν Ga40-O17 (17)
225	-	-	δ C18-C20-C25 (38), τ C22-C23-C24-C25(13)
207	-	-	
190	-	-	δ C18-C31-C34 (20), ν C8-C18 (16)
172	-	179 w	δ C18-C20-C25 (13), τ C7-C8-C9-O10(12)
163	-	-	δ C9-C8-C18 (14), δ C31-C34-C36 (10), δ C18-C31-C34 (12), νGa40-O17 (14)
150	-	143 w	τ C5-C4-O10-C9 (19), τ C4-O10-C9-C8(10), τ C18-C8-C9-O10(11), τ C7-C8-C9-O10(15)
122	-	-	τ H37-C36-C34-O35 (80)
102	-	-	τ C5-C4-O10-C9 (22), τ C8-C9-O17-Ga40 (12)

Table 4. *Cont.*

Scaled Wavenumber (cm^{-1})	Experimental Wavenumber (cm^{-1})		Vibrational Assignment with PED% (≥10)
	IR	Raman	
99	-	-	τ C4-O10-C9-C8(14), τC18-C8-C9-O10(14), τ C2-C3-C7-O15(13), τ C7-C8-C9-O10(13)
75	-	-	δ C9-C8-C18 (27), δC18-C31-C34 (14)
55	-	-	τ C31-C8-C20-C18(26)
50	-	-	δ C9-O17-Ga40 (15), τ C18-C31-C34-C36(10), τC20-C18-C31-C34(59)
38	-	-	δ C9-O17-Ga40 (14), τ C18-C31-C34-C36(46),
36	-	-	δ C9-O17-Ga40 (17),
32	-	-	τ C8-C18-C20-C25(57)
28	-	-	τ C8-C18-C20-C25(14)
21	-	-	τ C9-C8-C18-C20 (53), τ C8-C9-O17-Ga40 (20)

N—stretching; δ—bending; τ—torsion.

4.5.1. Coumarin Ring Vibrations

In hetero aromatic compounds, C-H vibrations remain in the frequency interval 3200–3000 cm^{-1} [28]. Weak-intensity bands appear at 3082 (Raman) and 3085 (IR) cm^{-1} and have been assigned to the C-H stretching mode. A series of bands identified at 1572 cm^{-1} (both IR and Raman), 1610 cm^{-1} (both IR and Raman), 1531 cm^{-1} (Raman), and 1404 cm^{-1} (Raman) have been attributed to C-C stretching vibration. Usually, the C-H in-plane bending vibrations occur as a number of strong to weak-intensity peaks in the region 1300–1000 cm^{-1} [29]. The C-H in-plane bending vibration appears as a weak-intensity band at 1278 (IR) and 1277 (Raman) cm^{-1}. The C-H out-of-plane bending vibration of the Ga(III) complex of warfarin appears as a weak-intensity peak at 951 (Raman), 952, and 899 cm^{-1} (IR).

4.5.2. Phenyl Ring Vibration

The phenyl ring C-H stretching vibrations are expected in the region 3120–3010 cm^{-1} [30]. The vibrational mode C-H stretching mode appears to be strongest in the Raman spectrum at 3061 cm^{-1}, and its counterpart is identified in the IR spectrum at 3062 cm^{-1}. C-H stretching mode appears both in the IR and Raman spectra, with weak intensities at 3032 and 3041 cm^{-1}, respectively. A strong IR band observed at 1618 cm^{-1} has been assigned to the C=C stretching mode. The C=C stretching mode is identified as a medium-intensity band at 1302 cm^{-1} in Raman and at 1307 cm^{-1} in IR as a weak-intensity band. For monosubstituted benzene, the C=C stretching mode appears in the regions 1515–1470 cm^{-1} and 1470–1440 cm^{-1}, respectively. This vibration C=C has a little C-H in-plane bending character, with carbon and its hydrogen moving oppositely. The C-C-H out-of-plane bending modes for the monosubstituted benzene are expected in the region 1000–650 cm^{-1}. Among the observed bands, the C-C-H out-of-plane mode has been identified at 919 (IR) and 918 (Raman) cm^{-1}. Medium-intensity bands observed at 1164 (IR) and 1159 (Raman) cm^{-1} have been assigned to the C-C-H out-of-plane mode of vibration.

4.5.3. Methyl and Methylene Vibrations

The CH_3 symmetric and asymmetric stretching modes usually appear at about 2965 and 2880 cm^{-1}, respectively [31]. In the Ga(III) complex of the warfarin molecule, the CH_3 symmetric mode has been observed as a strong-intensity IR band at 2904 cm^{-1}. Weak IR bands observed at 2995 and 2928 cm^{-1} and medium-intensity Raman bands identified at 2995 and 2931 cm^{-1} have been attributed to CH_3 asymmetric mode. Usually, the symmetric and asymmetric bending modes of the methyl group appear in the regions 1465–1440 cm^{-1} and 1390–1370 cm^{-1}, respectively [32]. A medium-intensity band observed at 1453 cm^{-1} in the IR spectrum has been assigned to CH_3 symmetric bending mode. The medium

band observed at 1378 cm^{-1} in IR and 1377 cm^{-1} in Raman has been assigned to CH_3 asymmetric bending mode.

The CH_2 asymmetric and symmetric stretching modes normally appear around 2926 and 2853 cm^{-1} [32]. The band observed at 2882 cm^{-1} in IR and 2885 cm^{-1} in Raman is due to CH_2 symmetric stretching mode. The wagging, twisting, and rocking modes appear in the region 1400–900 cm^{-1}. The bands at 1219 (both IR and Raman), 885 (IR), and 883 (Raman) cm^{-1} represent the unambiguous assignment of CH_2 twisting and rocking modes.

4.5.4. C=O, C-O, and O-H Stretching Vibrations

In cyclic ketones, the frequency of C=O stretching mode remains in the interval 1715–1680 cm^{-1} [32]. In this molecule, the C=O stretching mode is observed in IR at 1682 cm^{-1} as a strong band and in Raman at 1682 cm^{-1} as a medium-intensity band. A medium-intensity band at 1245 (IR) cm^{-1} and a weak-intensity band at 1242 (Raman) cm^{-1} have been assigned to C-O stretching vibration. A strong IR band observed at 3278 cm^{-1} has been assigned to O-H stretching mode.

4.6. HOMO and LUMO Energy Analysis

The energy of the HOMO is directly related to the ionization potential, and the energy of the LUMO is directly related to the electron affinity. The energy difference between the HOMO and LUMO orbitals is called the energy gap, which is an important stability factor for structures. The HOMO and LUMO energy level plots are shown in Figure 7. The HOMO–LUMO energy band gap value (ΔE) is 1.70 eV.

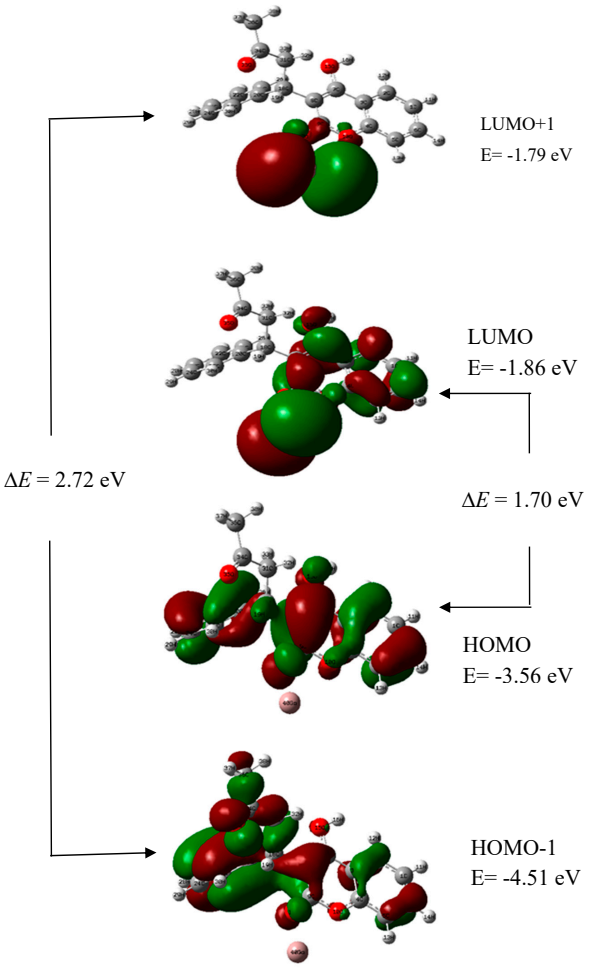


Figure 7. HOMO and LUMO orbital energy plots of the Ga(III) complex of warfarin.

4.7. Molecular Docking Analysis

Molecular docking provides insight into plausible protein-ligand interactions. A large number of research activities in pharmaceutical science are concentrated in the development of compounds that scan inhibit tyrosine kinase activity in the expectation that the potent and selective inhibitors would represent a new class of therapeutics for cancer as well as other proliferative diseases. Therefore, aurora-a kinase and tankyrase inhibitors can be applied suitably as a new mode of cancer therapy. The docking study of WG has been performed with three different proteins. The protein preparation has been carried out by the following steps: (i) all water molecules were removed; (ii) hydrogen atoms were added to the crystal structure; (iii) Kollman's charges were added; and (iv) previous docked inhibitors were removed from the protein. All the rigid proteins and flexible ligand dockings were performed using the AutoDock 4.2 program interfaced by AutoDock Tools 1.5.6rc30 using the Lamarckian genetic algorithm [33,34]. The WG was docked within the protein aurora kinase (PED IDs: 2C6E, 2C6D, 4L2K) [35,36]. As shown in Table 5, their AutoDock binding energy (ΔG) and inhibition constant (K_i) were obtained. Table 6 shows a summary of the hydrogen bonding of aurora with WG sites. The protein–ligand hydrogen bonding interaction diagrams are given in Figures 8–10. The docking study illustrated the affinity of the compound toward its target protein (4l2K) with a good binding energy value (-7.35 kcal mol^{-1}) and hence its suitability as a potential precursor to prepare new anticancer agents.

Table 5. Molecular docking results of the Ga(III) complex of warfarin with different target proteins.

Ligand	Target Proteins (PDB ID)	Estimated Inhibition Constant (K_i) (μM)	Binding Energy (kcal mol^{-1})
Warfarin gallium	2C6D	68.62 μM	–5.68
	2C6E	152.15 μM	–5.21
	4L2K	4.09 μM	–7.35

Table 6. Summary of hydrogen bonding of the WG molecule with different types of cancer protein targets.

Proteins [PDB ID]	Bounded Residues	No. of Hydrogen Bonds	Bond Distance (Å)	H-Bond Energy (kcal mol^{-1})
2C6D	protein:A:LEU261:CD1	4	2.6	–4.96
	protein:A:ASN260:HD2		2.3	–3.76
	protein:A:GLY275:HN		2.5	–3.99
	protein:A:SER277:HN		2.0	–1.93
2C6E	protein:A:GLY1132:O	1	2.0	–3.58
4L2K	protein:A:ASP993:HN	1	2.1	–3.57

The strength of the hydrogen bond X–H---Y is characterized by the X---Y distances. The hydrogen bonds corresponding to O–H distances may be 1.2 to 1.0 Å [37]. The shortening of O-H distances explores the strong hydrogen bonding interactions between the ligand and the target protein residues, which leads to the bioactivity of the molecule.

Based on the theoretical investigations, the most probable structure of the studied complex is presented in Figure 11.

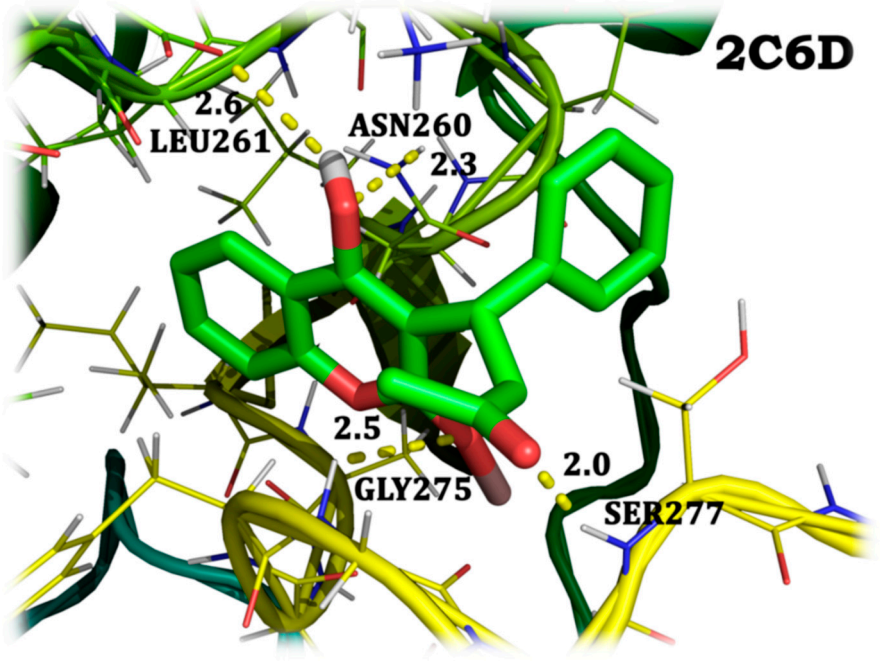


Figure 8. Docked conformation of ligand in the binding site of 2C6D along with distances (in Å) between amino acid residues.

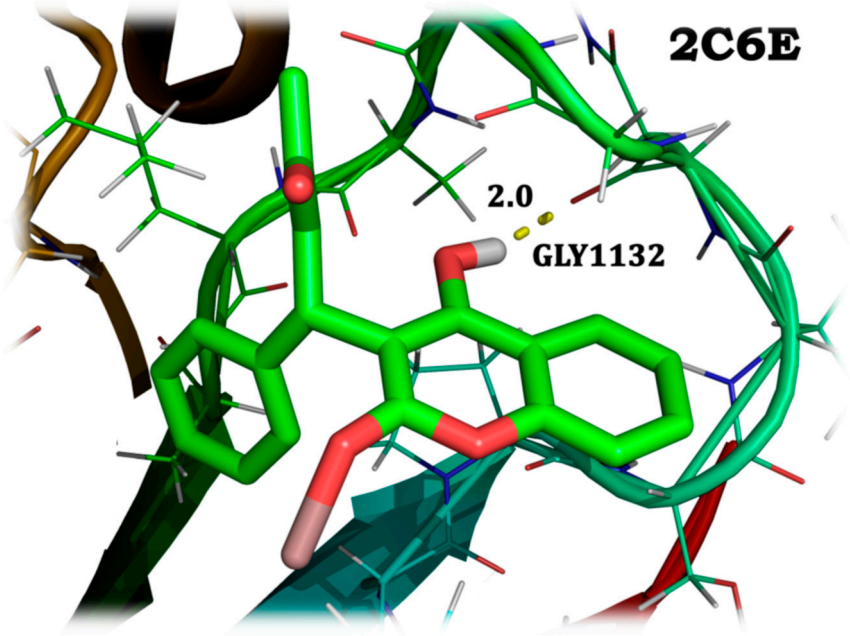


Figure 9. Docked conformation of ligand in the binding site of 2C6E along with distances (in Å) between amino acid residues.

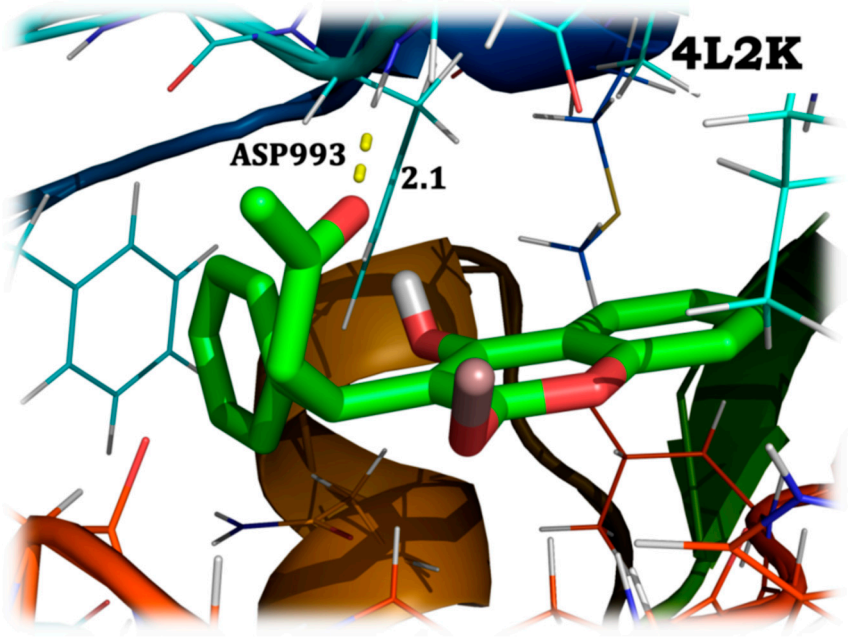


Figure 10. Docked conformation of ligand in the binding site of 4L2K along with distances (in Å) between amino acid residues.

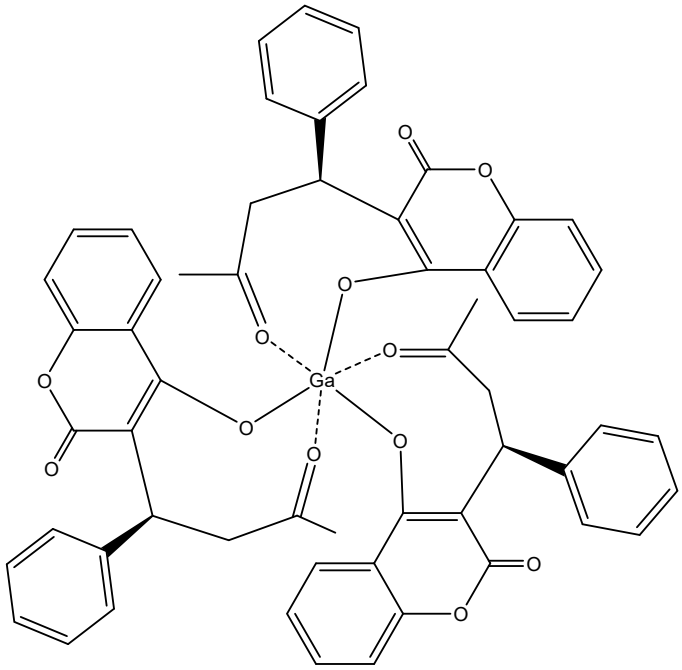


Figure 11. The most probable structure of the studied Ga(III) complex.

The study of the biological activity of the studied compounds is a practical upgrade of the applied theoretical approaches and physicochemical methodologies for the characterization of compounds, which enabled the output of useful structure-activity correlations, as applied by many strong research groups [38–42].

4.8. Pharmacology

The results of the preliminary cytotoxic screening of warfarin, sodium salt of warfarin, and the Ga(III) complex of warfarin are presented in Figure 12.

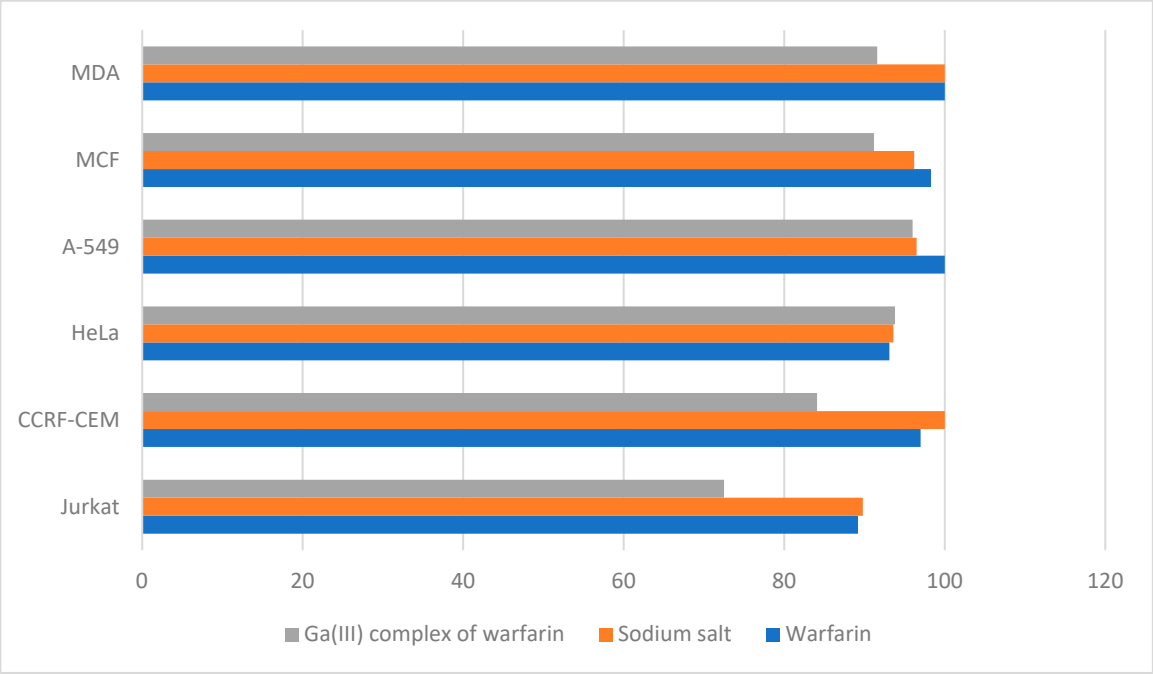


Figure 12. Cytotoxicity of studied compounds at a concentration of 10^{-4} mol.L^{-1} (percentage of living cells) compared to solvent control (100%).

The investigated compounds were tested for their cytotoxic activities on the Jurkat (human T-cell acute lymphoblastic leukemia), HeLa (human cervical adenocarcinoma), MCF-7 (human breast adenocarcinoma, estrogen receptor-positive), MDA-MB-231 (human breast adenocarcinoma, estrogen receptor-negative), A-549 (human lung adenocarcinoma), and CCRF-CEM (human T-cell acute lymphoblastic leukemia) cell lines. It has been observed that the exposure of Jurkat cells to 25 M cisplatin for 3 h has resulted in a significant loss in cell viability [43]. After 72 h of incubation, the degree of cytotoxicity on CCRF-CEM cells has shown 60–70% cell viability [44]. It has been found that about 81% of HeLa cells were killed by the combination of ZD55-IL-24 and 50 μM cisplatin for 72 h [45]. The cell viability of A549 cells has decreased ~2.00-fold when treated with 10 μM cisplatin [46]. The reduction in cell viability of MCF-7 and MDA-MB-231 cells at 10 and 20 μM cisplatin was around 58% and 45%, respectively [47]. The results obtained here indicate that the tested compounds exerted cytotoxic activity on the evaluated cell lines. The ligand (warfarin and the sodium salt of warfarin) exerted a very weak antiproliferative effect on these cells. This is in contrast to the Ga(III) complex of warfarin. The cytotoxicity of Ga ions is well known. These results confirmed our previous observations on the cytotoxicity of Ga(III) complexes with other biologically active ligands [48–50].

5. Conclusions

The coordination behavior of warfarin to Ga(III) and the DFT and vibrational (IR and Raman) analysis were discussed. Optimized structural studies of the molecule reveal the possibility of C-H---O intramolecular hydrogen bonding. NBO analysis proves the presence of conjugative, hyperconjugative, and intramolecular charge transfer interactions in the molecule. PED analysis has been used to assign the vibrational modes unambiguously. Simulated wavenumbers show good agreement with the experimental wavenumbers. The HOMO–LUMO energy gap describes the charge transfer taking place within the molecule, which is responsible for the improved chemical as well as biological activity of the molecule. The binding efficiency of WG was evaluated with target receptors of 2C6D, 2C6E, and 4L2K and it proved the strong hydrogen bonding interactions between protein and ligand complex, which led to its anticancer activity.

The results from the preliminary cytotoxic screening of warfarin, sodium salt of warfarin, and the Ga(III) complex demonstrate the antiproliferative potential of the Ga(III) complex, which is in line with our preceding papers concerning the activity of metal coordination compounds with diverse biologically active coumarins. The complex formation proved to be beneficial for the efficacy of the Ga(III) complex. Ga(III)-based compounds are promising antitumor agents, with the Ga(III) ion being responsible for the cytotoxicity. Bearing in mind the role of free radicals in carcinogenesis, the interaction of an antineoplastic agent with these radicals at physiological homeostatic conditions is of great importance and deserves to be investigated. If the antitumor agent is able to eliminate the free radicals, this can protect normal cells from malignization. Thus, it necessitates further, more detailed pharmacological evaluation.

Author Contributions: Methodology, V.A. and J.M.; Investigation, H.J.; Supervision, I.K. All authors contributed equally. All authors have read and agreed to the published version of the manuscript.

Funding: The financial support received by the European Union-Next Generation EU, through the National Recovery and Resilience Plan of the Republic of Bulgaria, project No. BG-RRP-2.004-0004-C01 is greatly acknowledged.

Data Availability Statement: The datasets used and analyzed during the current study are available from the corresponding author upon reasonable request.

Conflicts of Interest: The authors declare no conflicts of interest.

References

1. Kostova, I. Synthetic and Natural Coumarins as Cytotoxic Agents. *Curr. Med. Chem.-Anti-Cancer Agents* **2005**, *5*, 29–46. [CrossRef] [PubMed]
2. Mihaylov, T.; Trendafilova, N.; Georgieva, I.; Kostova, I. Coordination properties of warfarin towards Pr(III) predicted from DFT and FT-IR studies. *Chem. Phys.* **2010**, *374*, 37–45. [CrossRef]
3. Amalanathan, M.; Joe, I.H.; Kostova, I. Density Functional Theory Calculation and Vibrational Spectral Analysis of 4-Hydroxy-3-(3-Oxo-1-Phenylbutyl)-2H-1-Benzopyran-2-One. *J. Raman Spectrosc.* **2010**, *41*, 1076–1084. [CrossRef]
4. Kostova, I.; Amalanathan, M.; Joe, I.H. Molecular First Order Hyperpolarizability and Vibrational Spectral Investigation of Warfarin Sodium. *Chem. Phys.* **2010**, *378*, 88–102. [CrossRef]
5. Mandakmare, A.; Narwade, M. Complexing activity of coumarin dervatives. *Orient. J. Chem.* **1997**, *13*, 155–158.
6. Kostova, I.P.; Manolov, I.; Konstantinov, S.; Karaivanova, M. Synthesis, physicochemical characterisation and cytotoxic screening of new complexes of cerium, lanthanum and neodymium with Warfarin and Coumachlor sodium salts. *Eur. J. Med. Chem.* **1999**, *34*, 63–68. [CrossRef]
7. Kostova, I.; Manolov, I.; Karaivanova, M. Synthesis, Physicochemical Characterization, and Cytotoxic Screening of New Zirconium Complexes with Coumarin Derivatives. *Arch. Pharm.* **2001**, *334*, 157–162. [CrossRef]
8. Kostova, I.; Stefanova, T. Synthesis, Characterization and Cytotoxic/Cytostatic Activity of Sm(III) and Gd(III) Complexes. *J. Coord. Chem.* **2009**, *62*, 3187–3197. [CrossRef]
9. Collery, P.; Keppler, B.; Madoulet, C.; Desoize, B. Gallium in Cancer Treatment. *Crit. Rev. Oncol./Hematol.* **2002**, *42*, 283–296. [CrossRef]
10. Peng, X.X.; Gao, S.; Zhang, J.L. Gallium (III) complexes in cancer chemotherapy. *Eur. J. Inorg. Chem.* **2022**, *6*, e202100953. [CrossRef]
11. Kurtuldu, F.; Mutlu, N.; Boccaccini, A.R.; Galusek, D. Gallium containing bioactive materials: A review of anticancer, antibacterial, and osteogenic properties. *Bioact. Mater.* **2022**, *17*, 125–146. [CrossRef]
12. Pribisko, M.; Palmer, J.; Grubbs, R.H.; Gray, H.B.; Termini, J.; Lim, P. Cellular uptake and anticancer activity of carboxylated gallium corroles. *Proc. Natl. Acad. Sci. USA* **2016**, *113*, E2258–E2266. [CrossRef]
13. Cen, J.H.; Xie, Q.H.; Guo, G.H.; Xu, S.Y.; Liu, Z.Y.; Liao, Y.H.; Liu, H.Y. Construction of 5-Fluorouracil and Gallium Corrole Conjugates for Enhanced Photodynamic Therapy. *J. Med. Chem.* **2024**, *67*, 9054–9068. [CrossRef]
14. Ellahioui, Y.; Parashar, S.; Gómez-Ruiz, S. Anticancer Applications and Recent Investigations of Metallodrugs Based on Gallium, Tin and Titanium. *Inorganics* **2017**, *5*, 4. [CrossRef]
15. Chitambar, C.R. Gallium-containing anticancer compounds. *Future Med. Chem.* **2012**, *4*, 1257–1272. [CrossRef]
16. Chitambar, C.R.; Antholine, W.E. Iron-targeting antitumor activity of gallium compounds and novel insights into triapine®-metal complexes. *Antioxid. Redox Signal.* **2012**, *18*, 956–972. [CrossRef] [PubMed]
17. Chitambar, C.R.; Seligman, P.A. Effects of different transferrin forms on transferrin receptor expression, iron uptake and cellular proliferation of human leukemic HL60 cells: Mechanisms responsible for the specific cytotoxicity of transferrin-gallium. *J. Clin. Investig.* **1986**, *78*, 1538–1546. [CrossRef] [PubMed]

18. Foster, B.J.; Clagett-Carr, K.; Hoth, D.; Leyland-Jones, B. Gallium nitrate: The second metal with clinical activity. *Cancer Treat. Rep.* **1988**, *70*, 1311–1319.
19. Chitambar, C.R. Medical applications and toxicities of gallium compounds. *Int. J. Environ. Res. Public Health* **2010**, *7*, 2337–2361. [CrossRef] [PubMed]
20. Lessa, J.A.; Gabrieli, L.P.; Heloisa, B. Gallium complexes as new promising metallodrug candidates. *Inorg. Chim. Acta* **2012**, *393*, 53–63. [CrossRef]
21. Mosmann, T. Rapid Colorimetric Assay for Cellular Growth and Survival: Application to Proliferation and Cytotoxicity Assays. *J. Immunol. Methods* **1983**, *65*, 55–63. [CrossRef] [PubMed]
22. Becke, A.D. Density-Functional Thermochemistry. IV. A New Dynamical Correlation Functional and Implications for Exact-Exchange Mixing. *J. Chem. Phys.* **1996**, *104*, 1040–1046. [CrossRef]
23. Becke, A.D. Density-Functional Exchange-Energy Approximation with Correct Asymptotic Behavior. *Phys. Rev. A* **1988**, *38*, 3098–3100. [CrossRef] [PubMed]
24. Lee, C.; Yang, W.; Parr, R.G. Development of the Colle-Salvetti Correlation-Energy Formula into a Functional of the Electron Density. *Phys. Rev. B* **1988**, *37*, 785. [CrossRef] [PubMed]
25. Frisch, M.J.; Trucks, G.W.; Schlegel, H.B.; Scuseria, R.M.; Cheeseman, J.R.; Scalmani, G.; Barone, V.; Mennucci, B.P.; Nakatsuji, H.; Caricato, M.; et al. *Gaussian-09, Revision A.02*; Gaussian, Inc.: Wallingford, CT, USA, 2009.
26. Rauhut, G.; Pulay, P. Transferable Scaling Factors for Density Functional Derived Vibrational Force Fields. *J. Phys. Chem.* **1995**, *99*, 3093–3100. [CrossRef]
27. Pulay, P.; Fogarasi, G.; Pang, F.; Boggs, J.E. Systematic AB Initio Gradient Calculation of Molecular Geometries, Force Constants, and Dipole Moment Derivatives. *J. Am. Chem. Soc.* **1979**, *101*, 2550–2560. [CrossRef]
28. Varsányi, G. *Vibrational Spectra of Benzene Derivatives*; Academic Press: New York, NY, USA, 2012.
29. Colthup, N. *Introduction to Infrared and Raman Spectroscopy*; Academic Press: New York, NY, USA, 1990.
30. Tammer, M.G. Sokrates: Infrared and Raman Characteristic Group Frequencies: Tables and Charts. *Colloid Polym. Sci.* **2004**, *283*, 235. [CrossRef]
31. Silverstein, R.; Webster, F.X.; Kiemle, D.J. *Spectrometric Identification of Organic Compounds*; John Wiley & Sons: New York, NY, USA, 1998.
32. Smith, B. *Infrared Spectral Interpretation: A Systematic Approach*; CRC Press: New York, NY, USA, 1999.
33. Morris, G.M.; Goodsell, D.S.; Halliday, R.S.; Huey, R.; Hart, W.E.; Belew, R.K.; Olson, A.J. Automated Docking Using a Lamarckian Genetic Algorithm and an Empirical Binding Free Energy Function. *J. Comput. Chem.* **1998**, *19*, 1639–1662. [CrossRef]
34. Morris, G.M.; Huey, R.; Lindstrom, W.; Sanner, M.F.; Belew, R.K.; Goodsell, D.S.; Olson, A.J. AutoDock4 and AutoDockTools4: Automated Docking with Selective Receptor Flexibility. *J. Comput. Chem.* **2009**, *30*, 2785–2791. [CrossRef]
35. Heron, N.M.; Anderson, M.; Blowers, D.P.; Breed, J.; Eden, J.M.; Green, S.; Hill, G.B.; Johnson, T.; Jung, F.H.; McMiken, H.H.; et al. SAR and Inhibitor Complex Structure Determination of a Novel Class of Potent and Specific Aurora Kinase Inhibitors. *Bioorg. Med. Chem. Lett.* **2006**, *16*, 1320–1323. [CrossRef]
36. Narwal, M.; Koivunen, J.; Haikarainen, T.; Obaji, E.; Legala, O.E.; Venkannagari, H.; Joensuu, P.; Pihlajaniemi, T.; Lehtiö, L. Discovery of Tankyrase Inhibiting Flavones with Increased Potency and Isoenzyme Selectivity. *J. Med. Chem.* **2013**, *56*, 7880–7889. [CrossRef]
37. Jeffrey, G.; Jeffrey, G. *An Introduction to Hydrogen Bonding*; Oxford University Press: London, UK, 1997.
38. Avdović, E.H.; Antonijević, M.; Simijonović, D.; Roca, S.; Topić, D.V.; Grozdanić, N.; Marković, Z. Synthesis and Cytotoxicity Evaluation of Novel Coumarin–Palladium (II) Complexes against Human Cancer Cell Lines. *Pharmaceuticals* **2022**, *16*, 49. [CrossRef] [PubMed]
39. Avdović, E.H.; Petrović, I.P.; Stevanović, M.J.; Saso, L.; Marković, J.M.D.; Filipović, N.D.; Marković, Z.S. Synthesis and Biological Screening of New 4-Hydroxycoumarin Derivatives and Their Palladium (II) Complexes. *Oxidative Med. Cell. Longev.* **2021**, *2021*, 8849568. [CrossRef]
40. Pessoa, J.C.; Correia, I. Misinterpretations in evaluating interactions of vanadium complexes with proteins and other biological targets. *Inorganics* **2021**, *9*, 17. [CrossRef]
41. Dey, S.; Hollis, T.K. Accessing low-valent titanium CCC-NHC complexes: Toward nitrogen fixation. *Inorganics* **2021**, *9*, 15. [CrossRef]
42. Avdović, E.H.; Milanović, Ž.B.; Živanović, M.N.; Šeklić, D.S.; Radojević, I.D.; Čomić, L.R.; Marković, Z.S. Synthesis, spectroscopic characterization, biological activity, DFT and molecular docking study of novel 4-hydroxycoumarine derivatives and corresponding palladium (II) complexes. *Inorganica Chim. Acta* **2020**, *504*, 119465. [CrossRef]
43. Tacka, K.A.; Dabrowiak, J.C.; Goodisman, J.; Penefsky, H.S.; Souid, A.K. Effects of cisplatin on mitochondrial function in Jurkat cells. *Chem. Res. Toxicol.* **2004**, *17*, 1102–1111. [CrossRef]
44. Vascellari, S.; Valletta, E.; Perra, D.; Pinna, E.; Serra, A.; Isaia, F.; Pivetta, T. Cisplatin, glutathione and the third wheel: A copper-(1, 10-phenanthroline) complex modulates cisplatin–GSH interactions from antagonism to synergism in cancer cells resistant to cisplatin. *RSC Adv.* **2019**, *9*, 5362–5376. [CrossRef] [PubMed]
45. Wu, Y.M.; Zhang, K.J.; Yue, X.T.; Wang, Y.Q.; Yang, Y.; Li, G.C.; Wang, Y.G. Enhancement of tumor cell death by combining cisplatin with an oncolytic adenovirus carrying MDA-7/IL-24. *Acta Pharmacol. Sin.* **2009**, *30*, 467–477. [CrossRef]

46. Ray, R.; Al Khashali, H.; Haddad, B.; Wareham, J.; Coleman, K.L.; Alomari, D.; Evans, H.G. Regulation of cisplatin resistance in lung cancer cells by nicotine, BDNF, and a β-adrenergic receptor blocker. *Int. J. Mol. Sci.* **2022**, *23*, 12829. [CrossRef]
47. Prabhakaran, P.; Hassiotou, F.; Blancafort, P.; Filgueira, L. Cisplatin induces differentiation of breast cancer cells. *Front. Oncol.* **2013**, *3*, 134. [CrossRef] [PubMed]
48. Todorov, L.T.; Saso, L.; Benarous, K.; Traykova, M.L.; Linani, A.; Kostova, I. Synthesis, Structure and Impact of 5-Aminoorotic Acid and Its Complexes with Lanthanum(III) and Gallium(III) on the Activity of Xanthine Oxidase. *Molecules* **2021**, *26*, 4503. [CrossRef] [PubMed]
49. Todorov, L.T.; Traykova, M.L.; Saso, L.; Kostova, I. In Vitro Interaction of 5-Aminoorotic Acid and Its Gallium(III) Complex with Superoxide Radical, Generated by Two Model Systems. *Int. J. Mol. Sci.* **2020**, *21*, 8862. [CrossRef]
50. Todorov, L.T.; Kostova, I.; Traykova, M.L. Lanthanum, Gallium and their Impact on Oxidative Stress. *Curr. Med. Chem.* **2019**, *26*, 4280–4295. [CrossRef] [PubMed]

Disclaimer/Publisher's Note: The statements, opinions and data contained in all publications are solely those of the individual author(s) and contributor(s) and not of MDPI and/or the editor(s). MDPI and/or the editor(s) disclaim responsibility for any injury to people or property resulting from any ideas, methods, instructions or products referred to in the content.